NASA Technical Memorandum 79214

ELASTOHYDRODYNAMIC FILM THICKNESS MEASUREMENTS OF ARTIFICIALLY PRODUCED NONSMOOTH SURFACES

C. Cusano
University of Illinois
Urbana, Illinois

and

L. D. Wedeven
Lewis Research Center
Cleveland, Ohio

Prepared for the
Joint Lubrication Conference
cosponsored by the American Society of Lubrication Engineers
and the American Society of Mechanical Engineers
Dayton, Ohio, October 16-18, 1979

ELASTOHYDRODYNAMIC FILM THICKNESS MEASUREMENTS OF ARTIFICIALLY PRODUCED NONSMOOTH SURFACES

by

C. Cusano
University of Illinois
Urbana, Illinois

and

L. D. Wedeven
National Aeronautics and Space Administration
Lewis Research Center
Cleveland, Ohio

E-9977

ABSTRACT

Optical interferometry is used to measure the elastohydrodynamic (EHD) film thickness associated with artificially produced nonsmooth surfaces. The nonsmooth surfaces are produced by modifying the surfaces of highly-polished balls with irregularities in the form of multiple grooves and dents. By closely spacing these irregularities it is possible not only to produce depressions on the surface of the balls but also to generate pseudo asperities. The average "roughness" wavelength of this artificially-produced, nonsmooth, surface approximates the average fundamental roughness wavelength found on surfaces of some mechanical elements operating under concentrated contact. By comparing the measured film thickness profiles to the stylus traces of the irregularities, it was possible to observe the local deformations associated with micro-EHD pressure generation. In both pure rolling and pure sliding conditions the artificially-produced "asperities" are deformed and complete separation exists between them and the mating surface. Such findings demonstrate the importance of local surface topography and resulting micro-EHD effects on the film thickness between rough surfaces in concentrated contact. In addition, sliding data are presented which demonstrate a severe constriction, caused by the irregularities, at the exit of the Hertzian region.

INTRODUCTION

Fatigue failures of mechanical elements which operate in concentrated contacts are usually divided into subsurface- and surface-initiated failures. Failures caused by asperity interactions and by indigenous surface defects such as furrows and dents are generally designated as surface-initiated failures while those caused by subsurface inclusions are generally designated as subsurface-initiated failures. With the recognition of the importance of surface-initiated fatigue failures in recent years, there has been a growing interest in trying to understand the role the film parameter, Λ, plays in such failures. This parameter, defined as the ratio of the central film thickness to the combined roughness of the mating surfaces (h_o/σ), has been widely accepted as a measure of the degree of surface asperity interaction in EHD contacts. The surface distress caused by this interaction causes plastic deformation of the asperities and subsequent micropitting and microcracking of the mating surfaces. Because of the surface damage caused by asperity interaction and because of the influence of the central film thickness on the stress concentration around indigenous defects, it has been recognized that Λ is one of the parameters which influences fatigue life (1, 2).

Theoretical models for bearing fatigue life have been developed which can predict failures when Λ is relatively large. However, the wide scattering of available experimental data suggest that existing theoretical models cannot be used to fully explain failures for relatively low values of Λ (2, 3). This is mainly because, at low values of Λ, the surface roughness becomes intimately involved in the lubrication process and the parameter σ is not sufficient to completely describe the surface characteristics of the surfaces in contact. It can generally be stated that the effects of asperity interaction and indigenous defects on surface-initiated fatigue life of mechanical elements operating at low values of Λ or very thin films is not completely understood.

As a first step in trying to understand surface-initiated fatigue failures in EHD contacts it is imperative to know how asperities and indigenous defects such as dents and furrows behave as they pass through the conjunction region. Both analytical and experimental studies have been done to better understand this behavior. The stress concentration around an idealized furrow in EHD rolling contact has been analytically studied by Chiu and Liu (4) and EHD lubrication of idealized asperities has been

analytically investigated by Chow and Cheng (5) and Fowles (6-8). Among the more related experimental studies have been those of Jackson and Cameron (9), Wedeven (10), and Wedeven and Cusano (11). In reference (9) optical interferometry was used to study artificially-produced grooves on a polished ball under sliding conditions. The grooves, which were held stationary, were oriented in both the transverse and longitudinal directions relative to the sliding direction of a transparent surface so that the effects of directional properties of roughness on EHD lubrication could be studied. In reference (10) a debris dent was studied as it passed through the conjunction region under rolling conditions. As done in reference (9) these studies were done by means of optical interferometry. Unlike the artificially-produced defects studied in reference (9), the dent studied in reference (10) was formed naturally during previous testing. In reference (11) optical interferometry was also used to investigate the effects of artificially-produced dents and grooves, on highly-polished balls, on the EHD film thickness in Hertzian contact. The artificially-produced defects geometrically approximated actual furrows and dents found in bearings and gears. In references (10) and (11) qualitative conclusions were drawn, by observing the film thickness under both rolling and sliding conditions, concerning the effects of indigenous defects on fatigue failures.

Having qualitatively investigated surface-initiated fatigue failures caused by indigenous defects, one of the purposes of this paper is to more fully understand surface-initiated fatigue failures caused by asperity interactions. It should be noted that any two real (rough) surfaces can be simulated as the contact of a rough surface (with an equivalent combined roughness of the two surfaces) and a smooth surface. Thus, real surfaces could ideally be simulated by "roughening" a smooth ball and, by means of optical interferometry, analyze its contact against a smooth disk. In obtaining the data presented in this paper an attempt has been made to simulate a rough surface as much as possible without sacrificing the continuity of the fringes so that film thicknesses could be accurately determined. The "rough" surface was made by closely-spacing a series of artificially-produced grooves and dents on smooth balls. With such spacings both summits (formed by the built-up edges of two adjacent defects) and depressions are formed relative to the geometric smooth surface of the balls. The surface irregularities were observed under both rolling and sliding conditions

as they passed through the conjunction region. In addition, data will be presented which show very significant reductions in the film thickness on the trailing edge of the irregularities as they pass through the EHD outlet constriction region.

EXPERIMENTAL APPARATUS

As stated previously, film thickness measurements were made by using optical interferometry. The optical elastohydrodynamic apparatus is shown in figure 1 and described in detail elsewhere (12, 13). The basic components of the apparatus consist of a ball which rides against a transparent disk.

Fringes of very good visibility were obtained by using a 17-percent-reflecting layer of chromium on the bearing surface of the transparent disk. Interference measurements were made with wavelengths of two colors (red and green). These were obtained by using a special filter and a xenon flash lamp as a light source. The details of this system and its calibration are described more fully in references (14) and (15). All measurements were carried out at room temperature (23° C).

TEST MATERIALS

The test bearing specimens are shown in figure 2. The ball is 0.02063 meter in diameter and made of AISI 52100 steel. Its nominal surface roughness is better than 0.018 μm rms (0.7 μin.) and its hardness is approximately 65 R_c. Other mechanical properties are shown in table I. The transparent disk is 0.102 meter in diameter and made of sapphire. Its mechanical properties are also given in table I.

The test ball was supported by three bearings located in a lubricant reservoir shown in figure 2. The rotation of the support bearings continuously supplies lubricant to the test ball.

The tests were performed with a synthetic paraffinic oil that was designated by the manufacturer as XRM 109F3. The properties of the test fluid are given in table II.

FORMATION OF ARTIFICIAL, NONSMOOTH, SURFACES

Nonsmooth surfaces were obtained by artificially producing dents and grooves on highly-polished balls. Optical interferometry can be effectively used to obtain accurate film thickness measurements with these surfaces only if the surface around and

inside the dents and grooves is highly polished. Film thickness measurements on real surfaces, such as those found on gears and bearings, could not be easily made by means of optical interferometry because it would have been difficult to obtain visible and continuous fringes. This difficulty stems from the fact that, on such surfaces, the asperities are relatively steep-sloped and closely spaced, thus causing the fringes to merge or disappear because of the limited resolution of the microscope used to observe them.

The surface irregularities were produced by using conical- and wedge-shaped carbide tools. With such tools, many irregularities could be produced on the surface of the softer balls without altering the initial tip geometry of the tools. Before the irregularities were produced, the ground conical and wedge portions of the carbide tools were highly hand-polished by using a fine diamond compound. By polishing the tools it was found that their tip would deform the surface of the balls without tearing or roughening the surface, thus insuring visible fringes for film-thickness measurements.

A simple fixture was designed so that the grooves and dents could be accurately spaced on the surface of the highly polished ball. The sizes of the dents and grooves were controlled by the bluntness of the tools and the load used to produce them. The load was applied directly to the tools by means of weights, and the tools were guided to reduce positioning problems. To insure a series of geometrically uniform grooves or dents, it was essential that the weights be gradually brought into contact with the tools so that no impact loading took place between the weights and the tools.

As previously stated, closely-spaced, steep-sloped, asperities cannot be effectively studied by means of optical interferometry. Therefore, the artificially-produced irregularities are not as closely-spaced as the typical mean asperity spacing found on honed surfaces such as in ball bearing rings. However, the typical slopes of the irregularities are approximately the same as those found on such surfaces. The peak-to-peak height of the irregularities is generally higher than the dominant (fundamental) peak-to-peak height of the surface roughness found on honed bearing rings. It should be noted that for ground surfaces both the dominant asperity spacing and the corresponding peak-to-peak height are generally larger than those for honed surfaces. The asperity spacing and peak-to-peak height found in ground surfaces, there-

fore, more closely approximate the asperity spacing and peak-to-peak height of the artificially-produced irregularities. The mean asperity slope for ground surfaces would generally be larger than that of the irregularities.

Some of the more pertinent data on the artificially-produced irregularities are as follows: The slope varies from 2° to 3.5°, the asperity spacing varies from 30 μm to 60 μm with a mean of approximately 40 μm and the peak-to-peak height varies from 0.5 μm to 1.4 μm. These data can be compared to the data presented in reference (16) where, for unrun honed ball bearing rings, the rms slopes for tracings made across the lay varies from 1.9° to 4° and the mean asperity spacing varies from 3.5 μm to 10 μm. In the same reference the asperity spacing, for tracings across the lay, for an unrun ground ball bearing ring is given as 9 μm while the rms slope is given as 7°. For tracings taken along the lay, which may not be too accurate since the stylus may follow a valley or weave between valleys, the unrun ground ring had an asperity spacing of 49 μm and an rms slope of 0.5°. Limited data (taken at NASA Lewis) on ground gear teeth, for which the stylus tracings were taken along the curvature of the teeth, give a peak-to-peak height of approximately 1 μm, an average asperity spacing of 16 μm and an average slope of 5°. Thus, it is seen that the surface topography produced by the artificial irregularities is not drastically different than the fundamental roughness found in real surfaces. It should be emphasized, however, that the artificially-produced nonsmooth surface only has some features that are similar to real surfaces. It is not claimed that the artificial nonsmooth surfaces simulate real (rough) surfaces.

RESULTS

The surface irregularities were observed by taking high-speed single flash photomicrographs. A xenon flash lamp was synchronized with the ball rotation and could be delayed so that the irregularities could be photographed in various positions within the conjunction region. In describing single irregularities the terms "leading" and "trailing edges" of the irregularity will be used. By "leading edge" it is meant the first portion of the irregularity that enters the Hertzian region and by "trailing edge" it is meant the last portion of the irregularity that enters the Hertzian region.

The experimental results will be presented in the following form:

(1) Photomicrographs of interference fringes showing the surface irregularities in the conjunction region under dynamic conditions.

(2) Cross-sectional plots of the film thickness distribution inside and in the vicinity of the irregularities as observed from the photomicrographs.

(3) Stylus traces of the "undeformed" geometry of the irregularities. The purpose of these traces is to compare the "undeformed" geometry of the irregularities to the geometry of the same irregularities observed under dynamic conditions.

Multiple Dents Under Rolling and Sliding Conditions

Figure 3 shows two artificially-produced, closely-spaced, dents formed with a cone-shaped tungsten carbide tool. In figure 4 a stylus trace through the deepest portion of the dents is given. The smaller of the two dents is approximately 0.9 μm deep while the larger is approximately 1.4 μm deep. The maximum width of each dent is approximately 70 μm. The "asperity" summit, formed by the adjacent built-up edges of the depressions and measured from the geometric smooth surface of the ball, is approximately 0.23 μm.

The dents under rolling conditions, in two separate positions in the Hertzian region, are shown in figures 5(a) and (b). The corresponding film thickness profiles are shown in figures 6(a) and (b). The central film thickness for a smooth ball operating under the same rolling conditions is approximately 0.16 μm. From figure 6(b) it is seen that the stylus trace predicts "asperity" contact between the mating surfaces while the dynamic data show that there is complete separation between the surfaces.[1] "Asperity" contact is also predicted if one compares the measured "asperity" summit (0.23 μm) to the central film thickness (0.16 μm). From this comparison and

[1]Throughout this paper, the superposition of the stylus traces on the dynamic profiles were made by approximately matching the geometric smooth surface of the balls (as represented by the stylus traces) to the smooth surface film thicknesses given by the dynamic profiles at the inlet and outlet of the conjunction region.

from the fact that complete surface separation exists under dynamic conditions, it is clear that considerable deformation of the "asperity" takes place.

In figures 7(a) and (b) the same dents are shown under sliding conditions.[2] Plots of the film thickness profiles are shown in figures 8(a) and (b). The central film thickness for smooth surfaces under the same sliding conditions is approximately 0.16 μm. From figure 8(b) it is again seen that there is a significant deformation of the "asperity" and that complete separation of the surfaces exists.

Because of additional micro-EHD effects, the deformation under sliding conditions is more pronounced than under rolling conditions. This can be easily seen from figure 9 where the film thickness profiles under both sliding and rolling conditions are shown. In figures 7(b) and 8(b) it is seen that at the trailing edge of the small dent the film thickness is appreciably increased and a pressure "tail" is formed which is similar to that reported in reference (11). As reported in reference (11), this pressure "tail" progressively lags the dent as the dent travels through the Hertzian region. These observations indicate that the local micro-EHD events associated with surface defects are essentially governed by the local topography of the surface. That is, the local pressure generation around each defect seems to be independent of its neighbors.

In order to more fully explore the possibility of the interdependence of closely-spaced defects, six-closely-spaced dents were formed as shown in figure 10. The stylus trace of four of the dents is shown in figure 11. Figures 12(a) and (b) show these dents under rolling and sliding conditions, respectively. The film thickness profiles are shown in figures 13(a) and (b) and a comparison of the film thickness under rolling and sliding conditions is shown in figure 14. The results observed for the six dents are similar to those observed for the two dents. Again, the deformation of the "asperities" is more pronounced under pure sliding conditions than under pure rolling conditions and the pressure variations around each dent seems to be influenced only by the local surface topography around that dent.

---

[2]All the data presented in this paper under sliding conditions were obtained by holding the disk fixed while the ball was rotating.

Considering that there are large variations of pressures caused by diverging and converging wedges within and around the dents it seems reasonable to assume that cavitation might exist under sliding conditions. If cavitation does occur in a dent there may be a difficulty with flow continuity for the following dent which would lead to starvation. From the data obtained, however, no cavitation has been observed. It should be noted that even if some cavitation did exist it would be difficult to see for the size of the defects considered.

Multiple, Perpendicular, Grooves Under Rolling and Sliding Conditions

Figure 15 shows three closely-spaced grooves formed on a highly-polished ball with a wedge-shaped tungsten carbide tool. The depressions are deepest at their centers and the depth gradually decreases on both sides of the centers along the length of the depressions. Figure 16 shows the stylus trace through the deepest portion of these grooves. The width of each groove is approximately 40 μm and their peak-to-peak height is approximately 0.65 μm. The minimum "asperity" summit is approximately 0.2 μm for the left "asperity" and 0.18 μm for the right "asperity."

Figures 17(a) and (b) shows the grooves under rolling and sliding conditions, respectively. The corresponding film thickness profiles are shown in figures 18(a) and (b) and a comparison of the rolling and sliding film thicknesses is shown in figure 19. As with the dents, the central film thickness for smooth surfaces operating under the same conditions is 0.16 μm for both rolling and sliding conditions The results presented in figures 18(a) and (b) show that no surface separation at the "asperities" is predicted from the stylus trace while complete surface separation exists at the "asperities" under dynamic conditions. As with dents, the results show that the micro-EHD events are very local in nature. This is particularly true for rolling. As observed with "asperities" formed by a series of dents, "asperities" formed by a series of grooves deform much more under sliding than under rolling conditions as shown in figure 19.

Data not presented in this paper for brevity indicate that, as the central film thickness increases, there is a reduction in the deformation of the surface irregularities. As expected, these findings show that the behavior of multiple defects is simi-

lar to that of single defects (10,11) in that the stress concentration caused by the defects are gradually relieved as the central film thickness increases.

Multiple, Parallel, Grooves Under Rolling and Sliding Conditions

The grooves presented in figures 20 and 21 are oriented so that they are parallel to the direction of flow. These grooves are of practical significance since many bearing surfaces have a surface lay which is parallel to the direction of motion. The width of each groove is approximately 32 μm and the peak-to-peak height is approximately 0.5 μm The maximum "asperity" summit is approximately 0.18 μm for the left "asperity" and 0.13 μm for the right "asperity "

Figures 22(a) and (b) show the grooves in two separate locations in the Hertzian region under rolling conditions The film thickness profiles are shown in figures 23(a) and (b). Again, the central film thickness for a smooth ball under rolling conditions is 0.16 μm. The results given in figure 23(a) show spectacular micro-EHD events. The film thickness at the "asperities" between the grooves is much larger than the film thickness on the left of the left groove and on the right of the right groove. It is seen from this figure that the "asperity" contact predicted by the stylus trace does not occur and that the separation of the surfaces can occur under very severe conditions.

Figures 24(a) and (b) show the same grooves under sliding conditions. The film thickness profiles are shown in figures 25(a) and (b) with figure 25(a) also showing the stylus trace of the grooves Under the same sliding conditions, the central film thickness for smooth surfaces would again be 0.16 μm. Note that the film thickness distribution for rolling shown in figure 23(a) is almost identical to that of sliding shown in figure 25(a) This is contrary to what was observed when the grooves were oriented perpendicular to the direction of flow where substantial differences were observed between rolling and sliding conditions. For the case when the grooves were oriented in the direction of flow, there is comparatively little change in the geometry of the grooves in this direction as it passes through the Hertzian region so that the presence of sliding will not significantly alter the micro-EHD activity. Thus, for topographical features oriented in the direction of flow the micro-EHD action is confined to the inlet region for sliding as well as for rolling conditions

Irregularities in Exit Region Under Sliding Conditions

It is well known that at the exit region of an EHD contact a sudden sharp peak occurs in the pressure curve. In the neighborhood of this peak there is a reduction in the oil film thickness This reduction or constriction has to occur so that continuity of flow can be maintained. If no constriction existed the extremely high negative pressure gradient would force more fluid out of the Hertzian region than was coming in the region.

How indigenous defects and rough surfaces behave when they pass through the constriction is of practical interest from the standpoint of surface fatigue failures and possibly scuffing. A series of photomicrographs have been taken which show surface irregularities in the form of single and multiple dents and grooves in the constriction region of the Hertzian contact. These photomicrographs are shown in figures 26 to 30. The (a) part of the photomicrographs gives the irregularities near the inlet or central portion of the contact while the (b) part gives the corresponding irregularities in the exit region. By taking two photomicrographs a comparison can be made between the film thickness at the constriction with and without irregularities.

Figures 26 to 30 show that, under sliding conditions, the presence of irregularities result in a further reduction in the film thickness at the constriction region. For smooth surfaces, figure 26(a), shows a film thickness at the constriction of approximately 0.10 μm. When the dent is at the constriction, as shown in figure 26(b), the film thickness in the constriction region drops to approximately 0.05 μm. Similar reductions take place for the irregularities shown in figures 27 to 30. The reduction in film thickness takes place at the trailing edges of the irregularities. Some of this reduction is due to the built-up edge around the irregularities, but by observing both the leading and trailing edges of irregularities as they pass through the constriction region it is concluded that most of the reduction is caused by something other than the built-up edge. The most likely explanation for this reduction can be attributed to the fact that, because of their converging wedges, the trailing edges of the irregularities can generate pressures which are much larger than the Hertz pressure Because of these pressures, much larger negative pressure gradients than would normally exist

at the exit are present and thus, to maintain continuity of flow, there is an increased restriction on the outflow. In addition, the greater pressure gradient could increase the temperature around the constriction region which would result in thinner films.

Under rolling conditions, it has been frequently observed that surface initiated fatigue spalls originate at the trailing edges of debris dents (16,17). The reason why these spalls initiate at the trailing edges has been given in reference (10). Even though no experimental data have been found which demonstrate the initiation of scuffing failures at the trailing edges of indigenous defects, the data presented in this paper suggest that such failures are possible.

DISCUSSION

The lubrication of the artificially-produced irregularities studied in this paper have demonstrated the complex lubrication process that takes place when very thin films exist. In predicting asperity interactions of real surfaces it is usually assumed that such interaction takes place when the combined asperity height (or statistical representations of such height) exceeds the mean separation of the surfaces. Provided that a major part of the load is caused by the EHD action, the mean asperity separation between two rough surfaces is given (to a first approximation) by the film thickness which would exist between two smooth surfaces operating under the same conditions.

Partial EHD theories have been developed based on asperity interactions and associated asperity deformations to determine what proportion of the total load is carried by the asperities (18,19). In these theories the load supported by the asperities is primarily determined by the ratio of the central film thickness (based on smooth surfaces) to the combined roughness of the two surfaces, h_o/σ. In calculating this load it is assumed that there were no micro-EHD effects caused by the surface roughness. Initially, this appears to be a good assumption since it can be argued that the film thickness is generated in the inlet region where the surface separation can be quite large and the relative magnitude of the roughness is small. Such an argument, however, is only true if the characteristic wavelength and amplitude of the roughness is small compared to the dimensions of the inlet region. When the characteristic wavelength and amplitude are similar to the dimensions of the inlet region, the shape of the

inlet region is substantially changed. Since the shape of this region is an important ingredient in the generation of hydrodynamic pressure it will ultimately influence the resulting film thickness in the Hertzian contact.

For the data presented in tnis paper the ratio of the central film thickness to the height of the "asperity" summit is as low as 0.69 for both rolling and sliding. Under these conditions asperity contact would be predicted if no micro-EHD effects existed. However, a complete separation of the surfaces has been observed on all tests conducted. The data presented seem to indicate that micro-EHD events play an increasingly important role in the lubrication process as h_o/σ decreases. Since this lubrication process becomes exceedingly complex as h_o/σ decreases, it is understandable why fatigue data for small values of h_o/σ are not very reliable. This unreliability is mainly due to the fact that the parameters h_o and σ are not sufficient for describing the lubrication phenomena when very thin films exist. The roughness parameter σ is not sufficient since it has been demonstrated that the lubrication process, at the very minimum, is also influenced by such parameters as roughness orientation and asperity slope. The roughness orientation might also substantially change the parameter h_o. While h_o seems to be a reasonable parameter to use for localized defects such as dents and also for transverse roughness, it is questionable whether such a parameter should be used to determine mean surface separation when thin films exist and when longitudinal roughness is dominant such as in bearing rings. The data for grooves parallel to the flow indicate that the nominal film thickness can be much lower than the film thickness for smooth surfaces operating under the same conditions. Such reductions of film thickness is due to the side leakage that occur as the grooves pass through the inlet region.

CONCLUSIONS

Some of the more important observations which can be made as the result of this study are:

1. The surfaces of highly-polished balls can be artificially modified with irregularities which are spaced at approximately the fundamental wavelength of some real (rough) surfaces.

2. A comparison between the film thickness measurements in the vicinity of and inside the irregularities to the stylus traces of the irregularities shows that significant deformations of the "asperities" occur.

3. For all the data presented, complete separation of the surfaces (at the "asperities") exists even though such separation would not be predicted by comparing almost all of the asperity summits to the central film thickness for a smooth surface.

4. The deformation of the "asperities" is more pronounced under sliding conditions than under rolling conditions with the exception of grooves oriented parallel to the flow where the "asperity" deformation is approximately the same for both sliding and rolling.

5. As the central film thickness decreases the micro-EHD effects caused by the irregularities become more dominant and these effects can substantially change the localized film thickness.

6. The changes in film thickness caused by each irregularity seem to be independent of neighboring irregularities especially under rolling conditions.

7. It has been demonstrated that the parameter h_o/σ, often used to predict asperity interactions, is not sufficient for describing the lubrication process when very thin films exist.

8. An appreciable reduction in the film thickness in the trailing edges of surface irregularities takes place under sliding conditions as the irregularities pass through the constriction region of the Hertzian contact.

ACKNOWLEDGMENT

The authors would like to thank Tom Morrell who meticulously measured the profiles of the irregularities and plotted their shapes from the interference fringes.

REFERENCES

1. Tallian, T. E., and McCool, J. I., "An Engineering Model of Spalling Fatigue Failure in Rolling Contact, II. The Surface Model," Wear, 17, 447-461 (1971).

2. Liu, J. Y., Tallian, T. E., and McCool, J. I., "Dependence of Bearing Fatigue Life on Film Thickness to Surface Roughness Ratio," Trans. ASLE, 18 (2), 144-152 (1975).

3. Li, D. F., Kauzlarich, J. J., and Jamison, W. E., "Surface Roughness Effects on Fatigue in Partial EHD Lubrication," J. Lubr. Technol., ASME Trans., 98, Series F (4), 530-537 (1976).

4. Chiu, Y. P., and Liu, J. Y., "An Analytical Study of the Stress Concentration Around a Furrow Shaped Surface Defect in Rolling Contact," J. Lubr. Technol., ASME Trans., 92, Series F (2), 258-263 (1970).

5. Chow, L. S. H., and Cheng, H. S., "Pressure Perturbation in EHD Contacts Due to an Ellipsoidal Asperity," J. Lubr. Technol., ASME Trans., 98, Series F (1), 8-15 (1976).

6. Fowles, P. E., "The Application of Elastohydrodynamic Lubrication heory to Individual Asperity-Asperity Collisions," J. Lubr. Technol. ASME Trans., 91, Series F (3), 464-476 (1969).

7. Fowles, P. E., "A Thermal Elastohydrodynamic Theory for Individual Asperity-Asperity Collisions," J. Lubr. Technol., ASME Trans., 93, Series F (3), 383-397 (1971).

8. Fowles, P. E., "Extension of the Elastohydrodynamic Theory of Individual Asperity-Asperity Collisions to the Second Half of the Collision," J. Lubr. Technol., ASME Trans., 93, Series F (2), 213-215 (1971).

9. Jackson, A., and Cameron, A., "An Interferometric Study of the EHL of Rough Surfaces," ASLE Trans., 19 (1), 50-60 (1976).

10. Wedeven, L. D., "Influence of Debris Dent on EHD Lubrication," ASLE Trans., 21 (1), 41-52 (1978).

11. Wedeven, L. D., and Cusano, C., "Elastohydrodynamic Film Thickness Measurements of Artificially Produced Surface Dents and Grooves," Presented at the ASME-ASLE Joint Lubrication Conference, Minneapolis, Minn., Oct. 24-26, 1978, ASLE Preprint No. 78-LC-1A-1.

12. Wedeven, L. D., "Traction and Film Thickness Measurements Under Starved Elastohydrodynamic Conditions," J. Lubr. Technol., ASME Trans., 97, Series F (2), 321-329 (1975).

13. Wedeven, L. D., "Effect of Starvation on Film Thickness and Traction Under Elastohydrodynamic Rolling and Sliding Conditions," NASA TN D-8087, 1975.

14. Wedeven, L. D., Evans, D., and Cameron, A., "Optical Analysis of Ball Bearing Starvation," J. Lubr. Technol., ASME Trans., 93, Series F (3) 349-363 (1971).

15. Foord, C. A., Wedeven, L. D., Westlake, F. J., and Cameron, A., "Optical Elastohydrodynamics," Proc. Inst. Mech. Eng., 184, pt. 1 (28), 487-505 (1969-1970).

16. Littmann, W. E., and Widner, R. L., "Propagation of Contact Fatigue from Surface and Subsurface Origins," Trans. of ASME, Journal of Basic Engineering, Sept. 1966, pp. 624-636

17. Martin, J. A., and Eberhardt, A. D., "Identification of Potential Failure Nuclei in Rolling Contact Fatigue," Trans. of ASME, Journal of Basic Engineering, Vol. 89, Dec. 1967, pp. 932-942.

18. Tallian, T. E., "The Theory of Partial Elastohydrodynamic Contacts," Wear, 21, 49-101 (1972)

19. Johnson, K. L., Greenwood, J. A., and Poon, S. Y., "Simple Theory of Asperity Contact in Elastohydrodynamic Lubrication," Wear, 19, 91-108 (1972).

TABLE I. - BEARING MATERIAL PROPERTIES

	Ball	Disk
Material	52100 Steel	Sapphire
Compressive strength	1.4×10^9 N/m^2	2×10^9 N/m^2
Elastic modulus	204×10^9 N/m^2	365×10^9 N/m^2
Poisson's ratio	0.3	0.25
Hardness	65 R_c	9 Moh
Roughness	0.018 μm rms	Optical polish

TABLE II. - PROPERTIES OF TEST FLUID

	Synthetic paraffinic oil (XRM 109F3)
Viscosity	45 830 cS at 17.8° C
	493 cS at 37.8° C
	42.6 cS at 98.9° C
Density	0.8389 g/cm^3 at 37.8° C
	0.8082 g/cm^3 at 93.3° C
	0.777 g/cm^3 at 149° C
Pressure viscosity coefficient	1.77×10^{-8} m^2/N at 37.8° C
	1.51×10^{-8} m^2/N at 99° C
	1.09×10^{-8} m^2/N at 149° C
Refractive index	1.4689 at 23° C

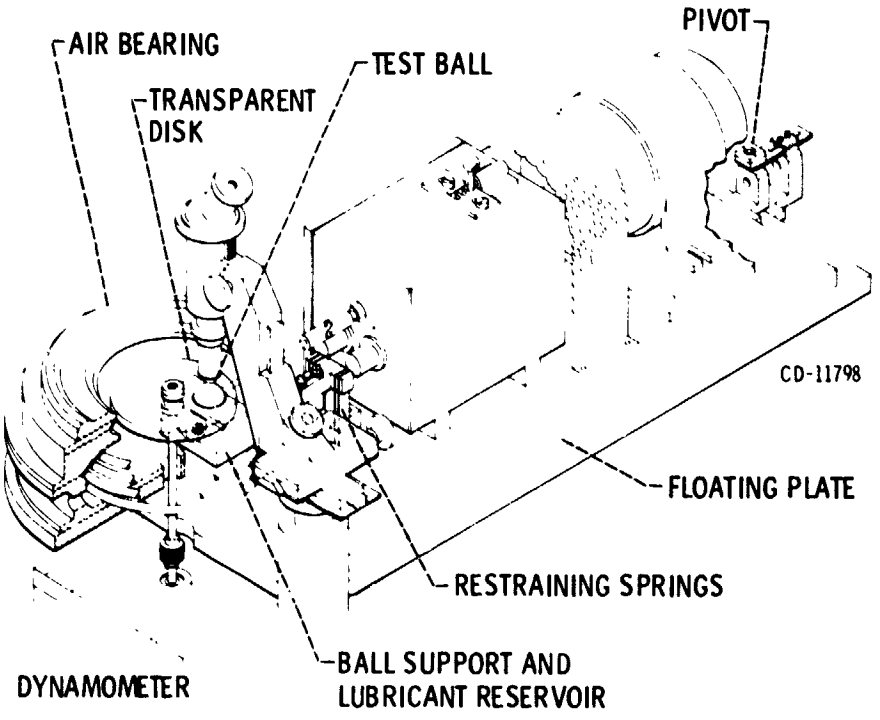

Figure 1. - Optical EHD rig.

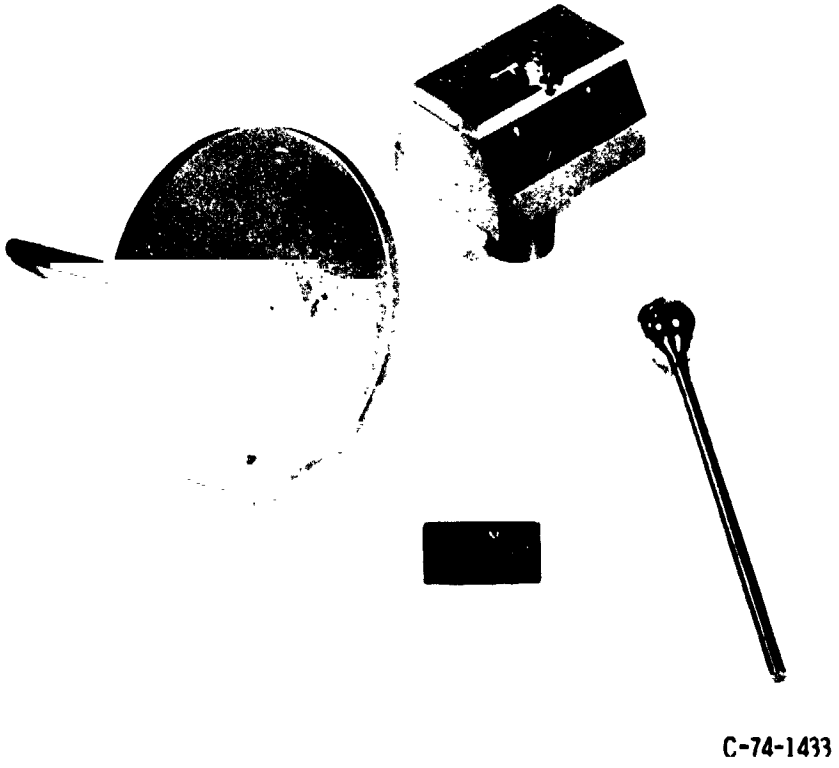

Figure 2. - Test ball, transparent disk and lubricant reservoir.

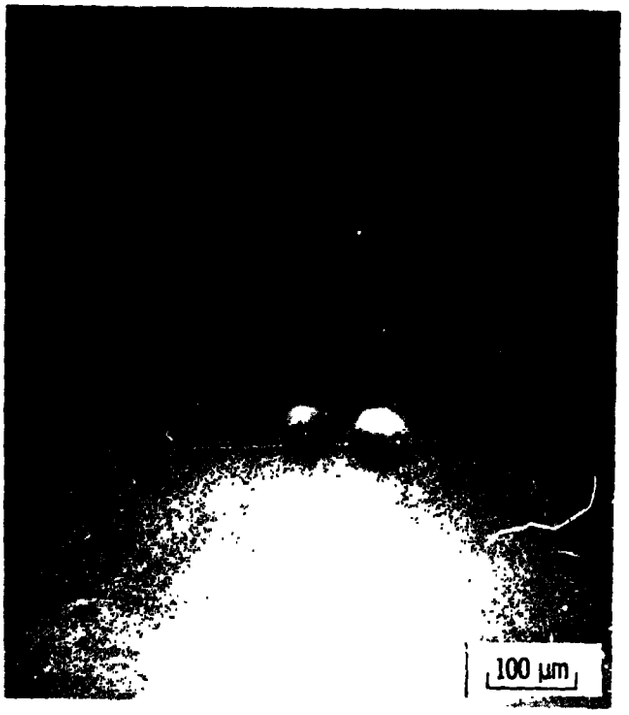

Figure 3. - Dents made with cone-shaped tool.

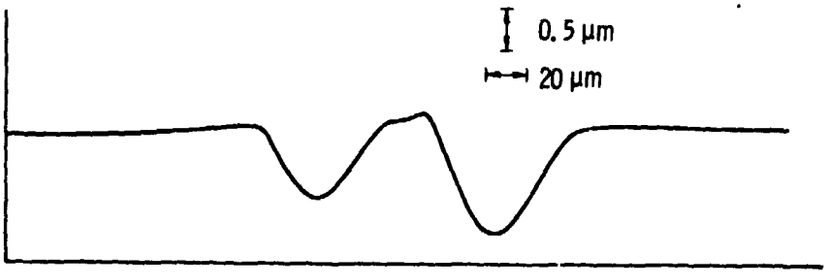

Figure 4. - Stylus trace of dents shown in figure 3.

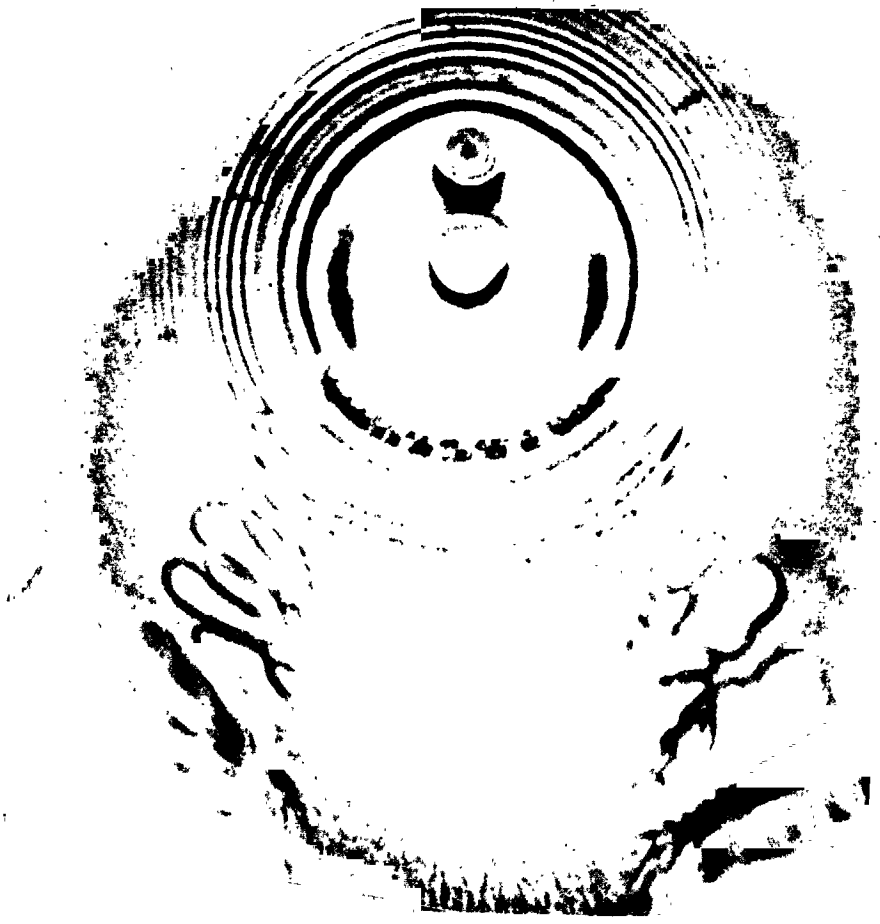

(a) PHOTOMICROGRAPH OF DENTS UNDER ROLLING CONDITIONS, DENTS NEAR INLET. $U = 0.0134$ M/S, $P_{max} = 1.13 \times 10^9$ N/M^2.

Figure 5.

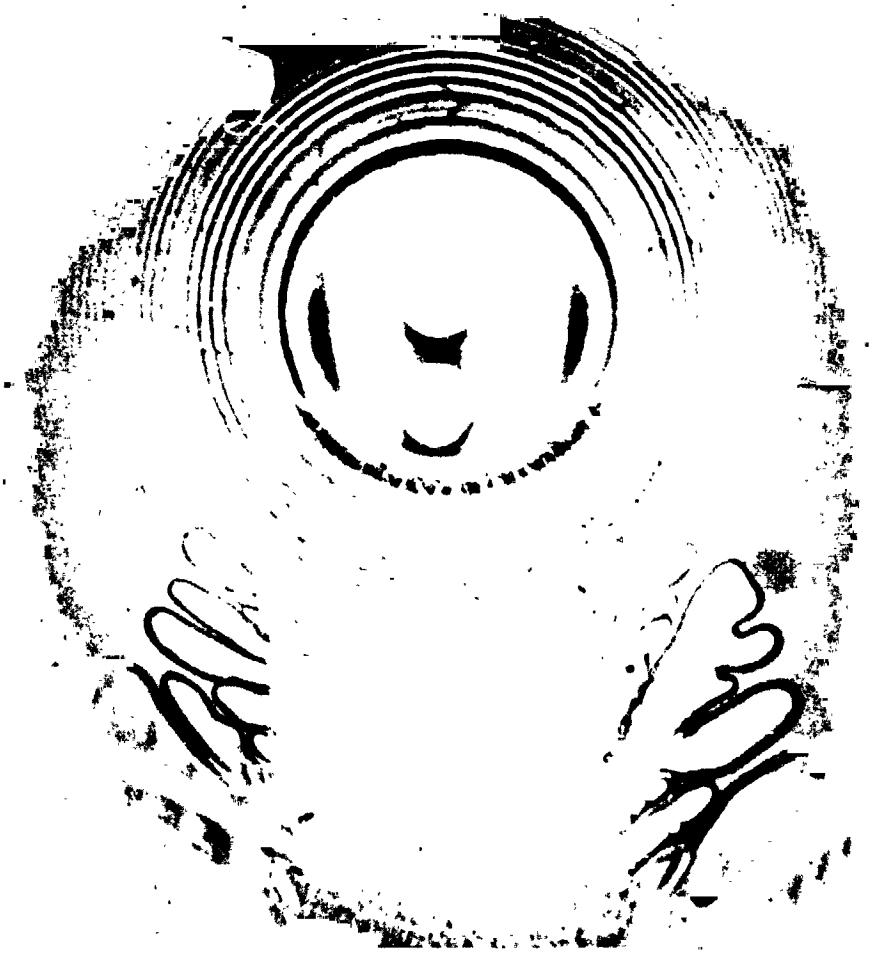

(b) PHOTOMICROGRAPH OF DENTS UNDER ROLLING CONDITIONS, DENTS NEAR EXIT. $U = 0.0134$ M/S, $P_{max} = 1.13 \times 10^9$ N/M^2.

Figure 5. - Concluded.

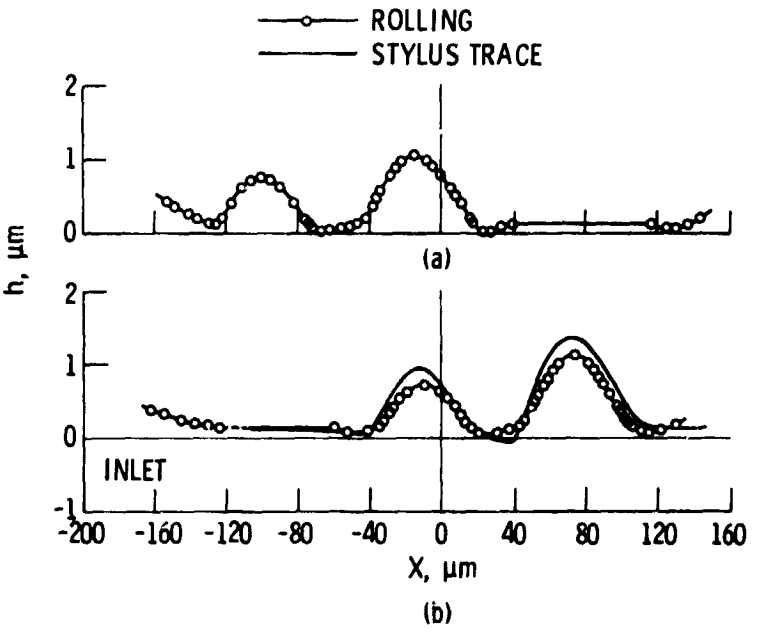

Figure 6. - (a) Measured profile of figure 5(a), (b) Comparison of measured profile of figure 5(b) and stylus trace.

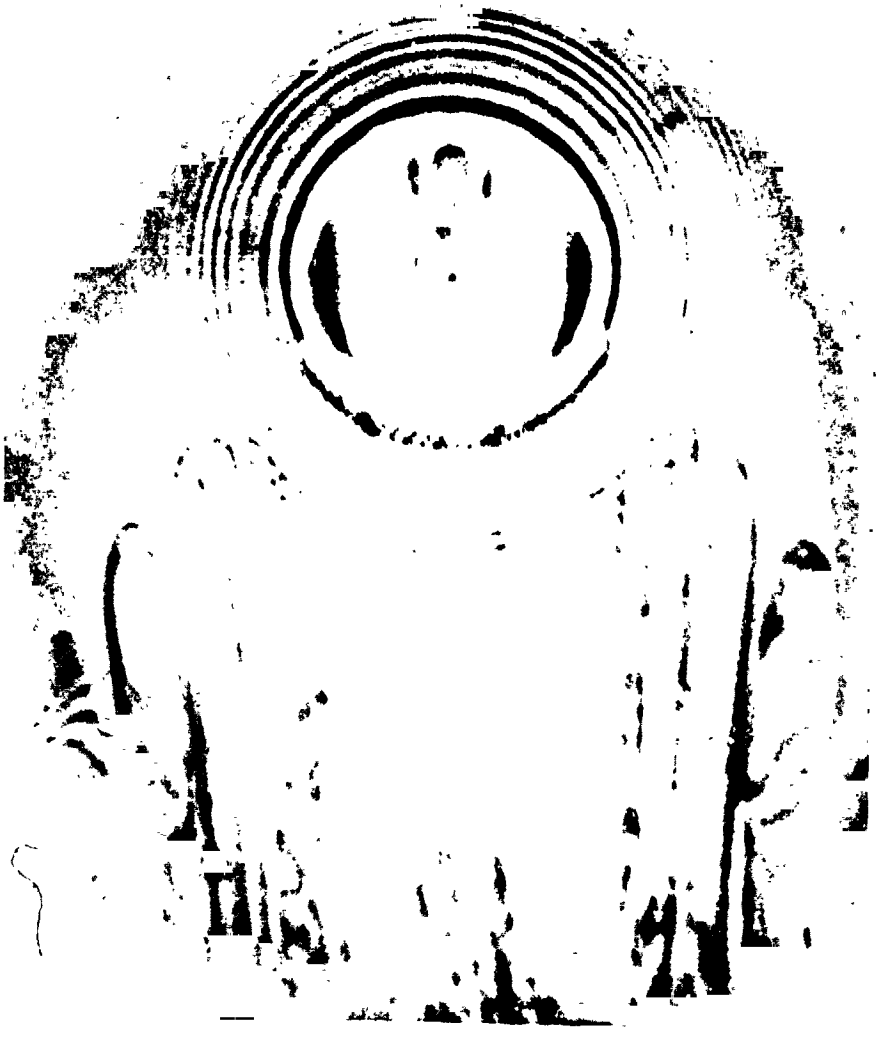

(a) PHOTOMICROGRAPH OF DENTS UNDER SLIDING CONDITIONS, DENTS NEAR INLET. $U = 0.0134$ M/S, $P_{max} = 1.13 \times 10^9$ N/M^2.

Figure 7.

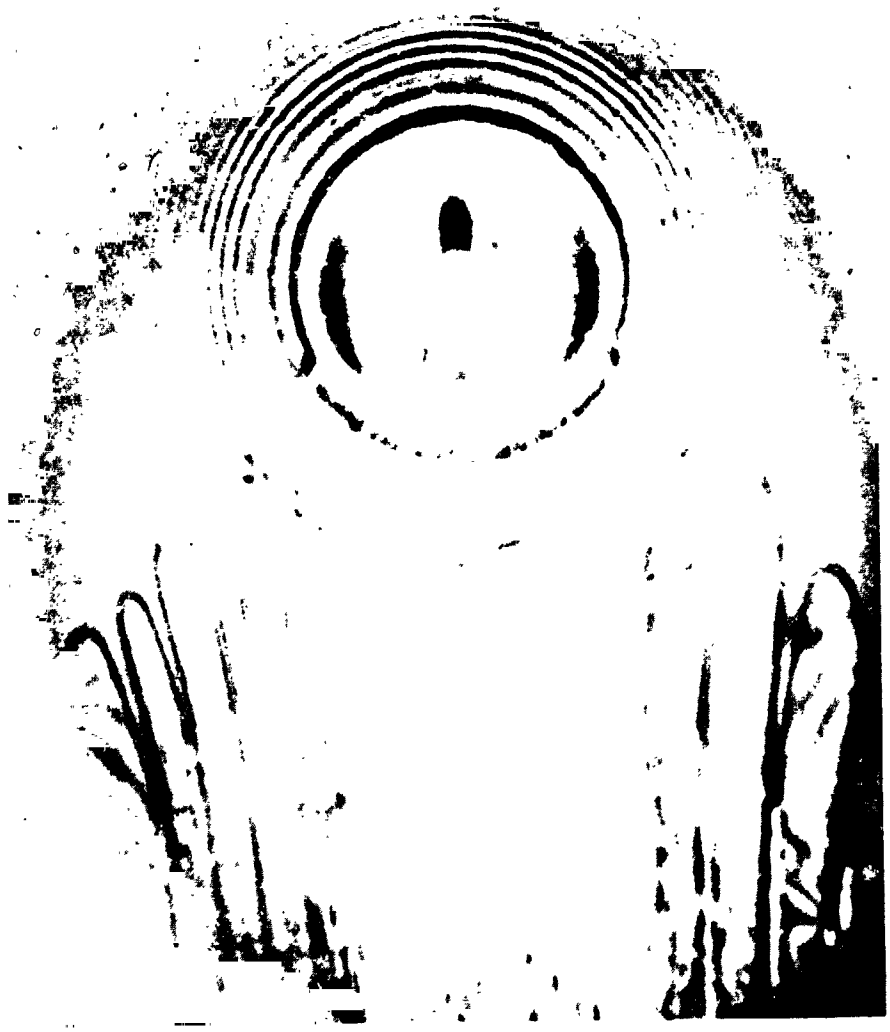

(b) PHOTOMICROGRAPH OF DENTS UNDER SLIDING CONDITIONS, DENTS NEAR EXIT. $U = 0.0134$ M/S, $P_{max} = 1.13 \times 10^9$ N/M^2.

Figure 7. - Concluded.

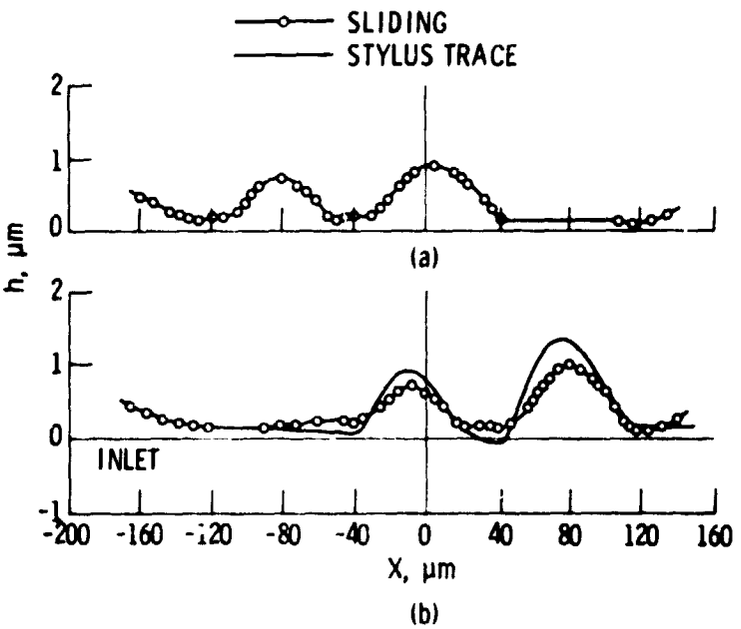

Figure 8. - (a) Measured profile of figure 7(a), (b) Comparison of measured profile of figure 7(b) and stylus trace.

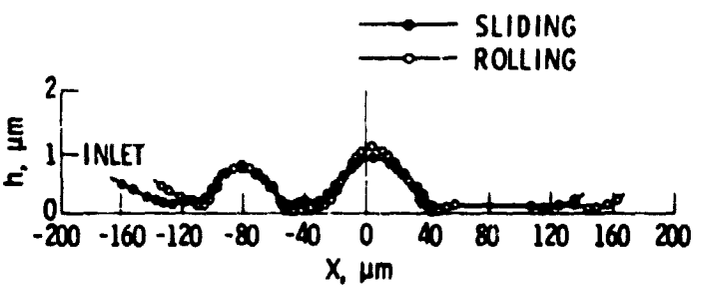

Figure 9. - Comparison of measured profiles under rolling and sliding conditions.

Figure 10. - Series of dents made with cone-shaped tool.

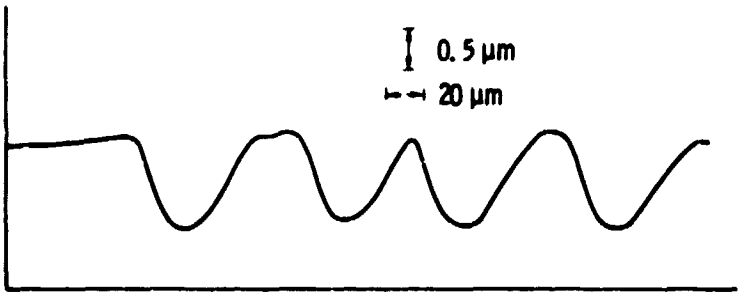

Figure 11. - Stylus trace of dents shown in figure 10.

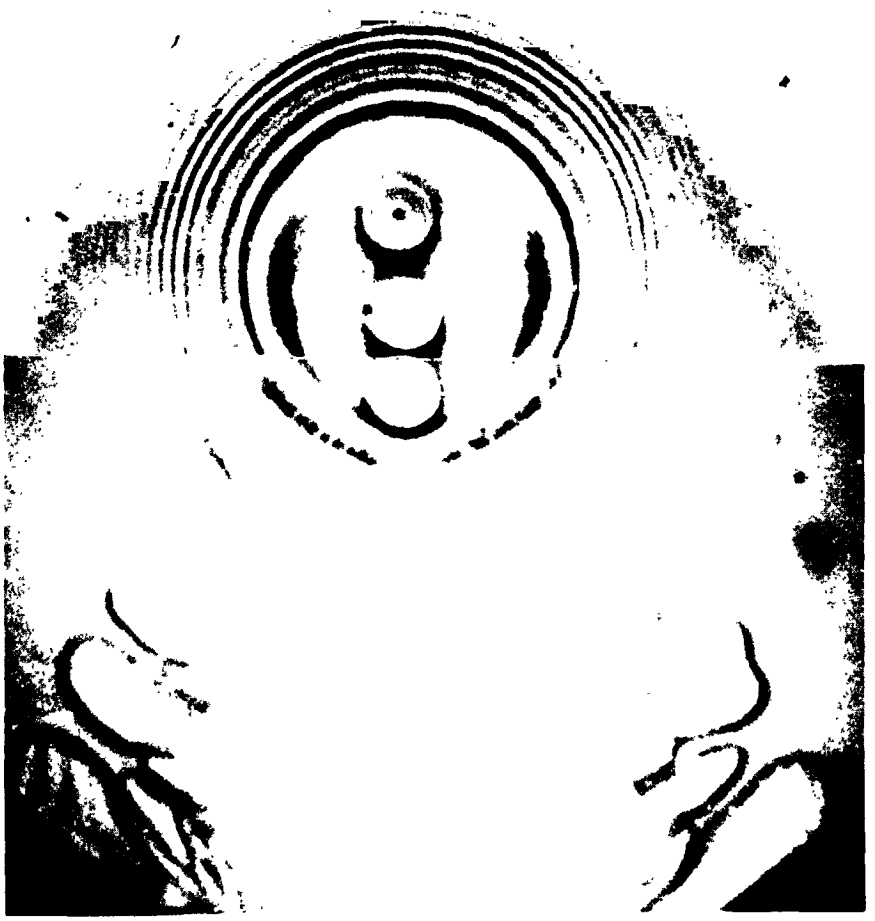

(a) PHOTOMICROGRAPH OF DENTS UNDER ROLLING CONDITIONS, U = 0.0134 M/S, $P_{max} = 1.13 \times 10^9$ N/M^2.

Figure 12.

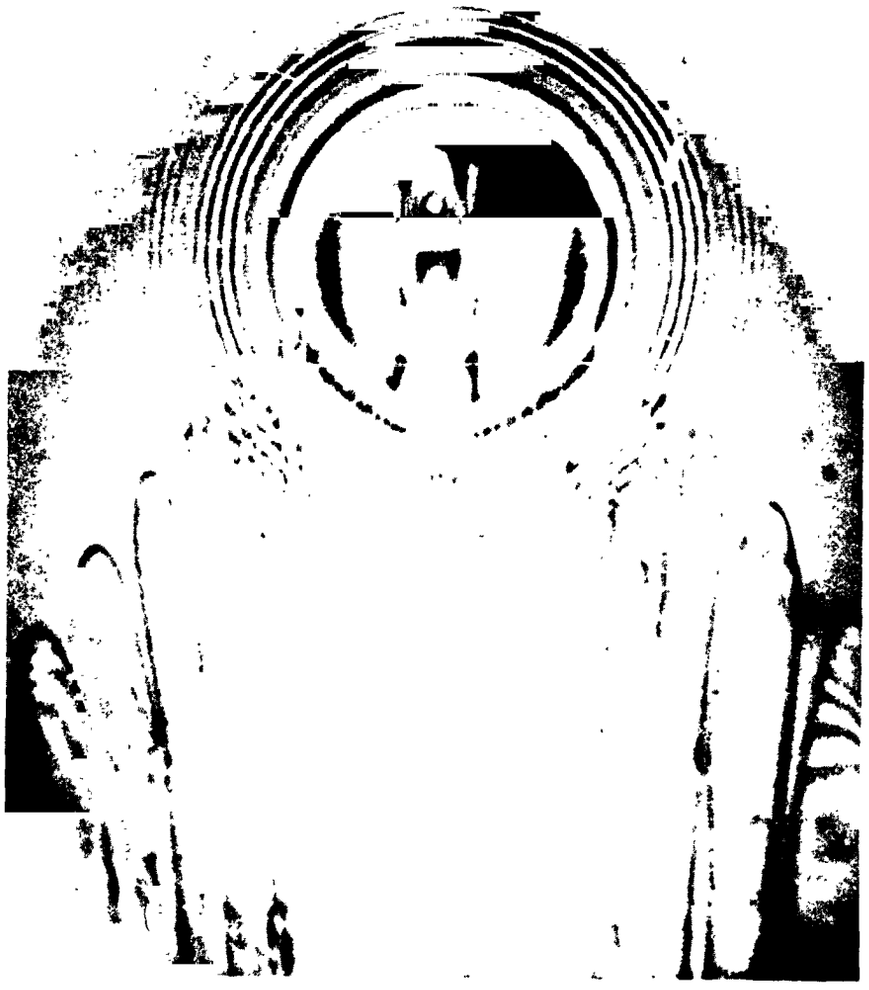

(b) PHOTOMICROGRAPH OF DENTS UNDER SLIDING CONDITIONS. U = 0.0134 M/S, $P_{max} = 1.13 \times 10^9$ N/M^2.

Figure 12. - Concluded.

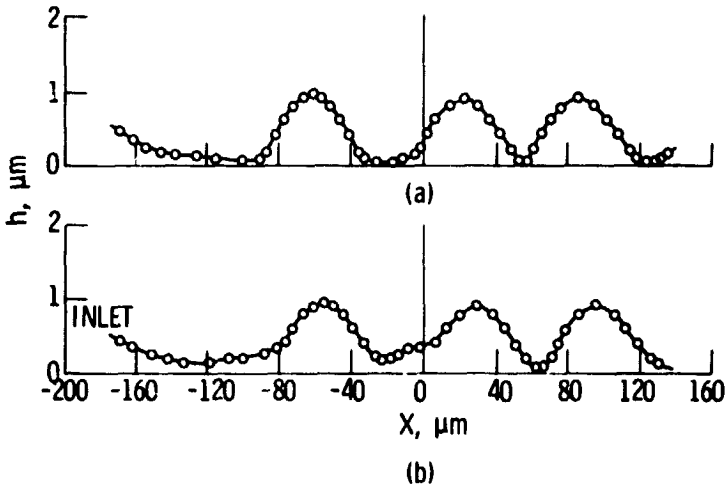

Figure 13. - (a) Measured profile of figure 12(a), (b) Measured profile of figure 12(b).

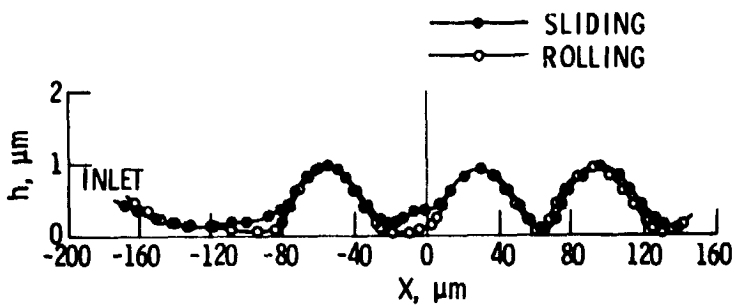

Figure 14. - Comparison of measured profiles under rolling and sliding conditions.

Figure 15. - Grooves made with wedge-shaped tool - perpendicular to direction of flow.

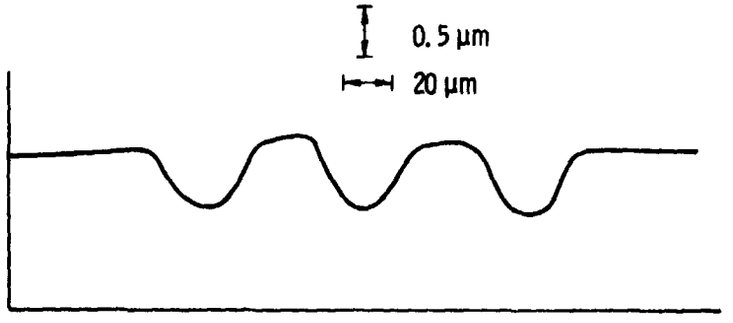

Figure 16. - Stylus trace of grooves in figure 15.

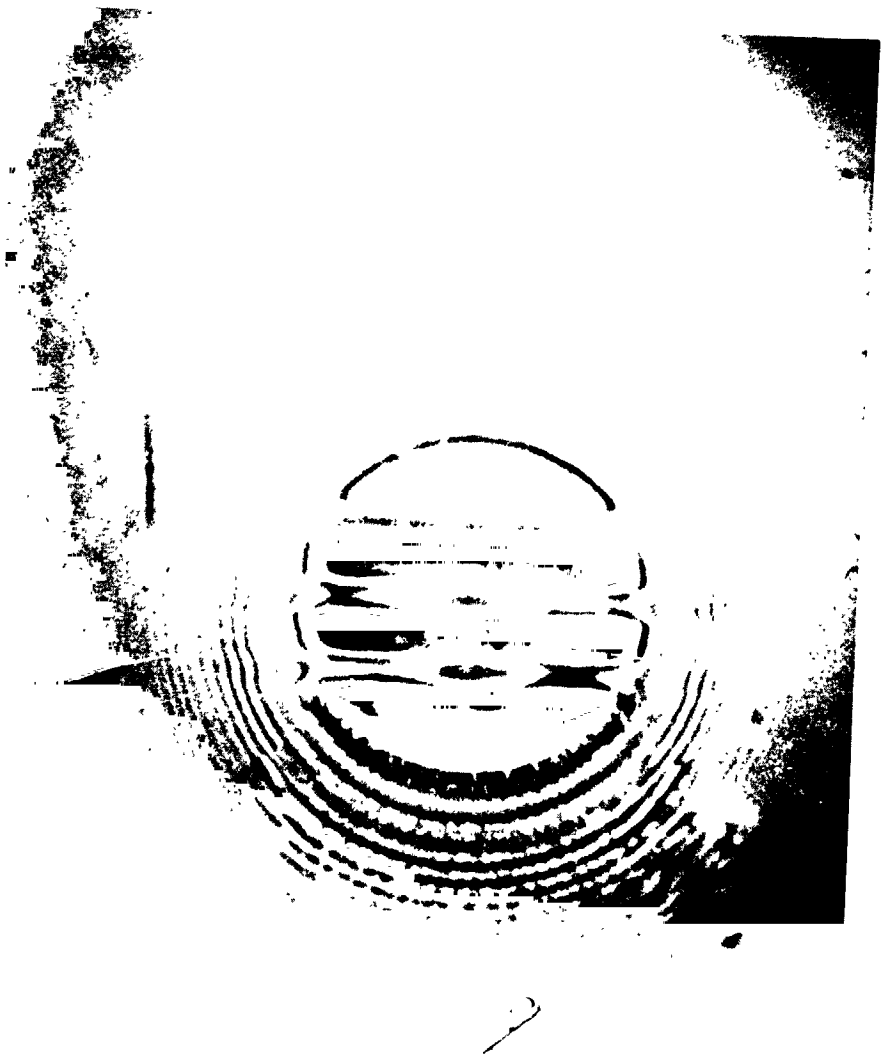

(a) PHOTOMICROGRAPH OF GROOVES UNDER ROLLING CONDITIONS. U = 0.0134 M/S, $P_{max} = 1.13 \times 10^9$ N/M^2.

Figure 17.

(b) PHOTOMICROGRAPH OF GROOVES UNDER SLIDING CONDITIONS. U = 0.0134 M/S, $P_{max} = 1.13 \times 10^9$ N/M^2.

Figure 17. - Concluded.

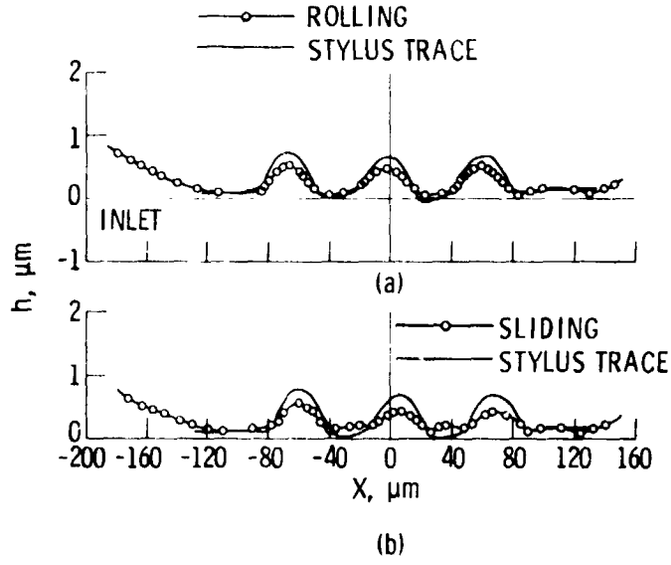

Figure 18. - (a) Comparison of measured profile of figure 17(a) and stylus trace, (b) Comparison of measured profile of figure 17(b) and stylus trace.

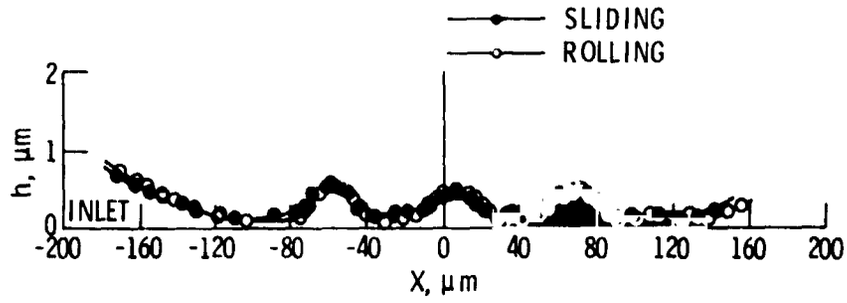

Figure 19. - Comparison of measured profiles under rolling and sliding conditions.

Figure 20. - Grooves made with wedge-shaped tool - parallel to direction of flow.

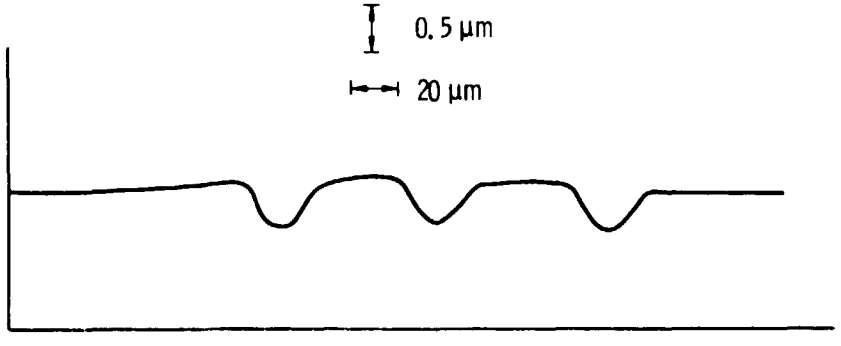

Figure 21. - Stylus trace of grooves in figure 20.

(a) PHOTOMICROGRAPH OF GROOVES UNDER ROLLING CONDITIONS, GROOVES NEAR CENTER. $U = 0.0134$ M/S, $P_{max} = 1.13 \times 10^9$ N/M^2.

Figure 22.

(b) PHOTOMICROGRAPH OF GROOVES UNDER ROLLING CONDITIONS, GROOVES NEAR EXIT. $U = 0.0134$ M/S, $P_{max} = 1.13 \times 10^9$ N/M^2.

Figure 22. - Concluded.

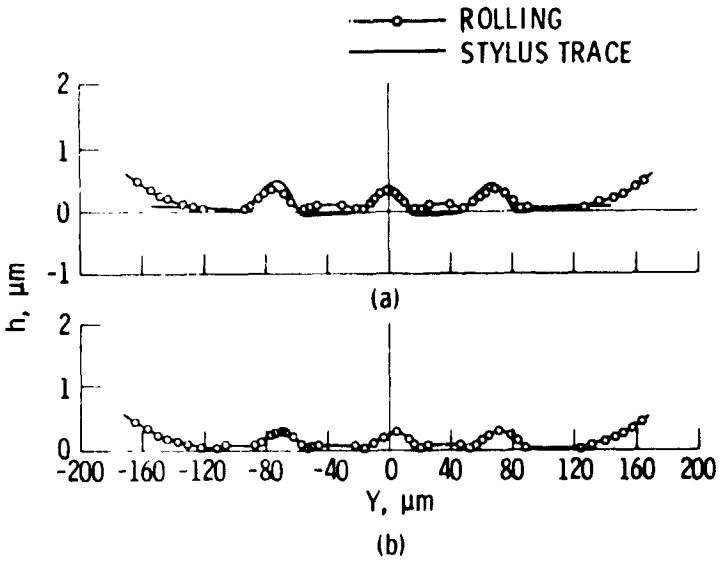

Figure 23. - (a) Comparison of measured profile of figure 22(a) and stylus trace, (b) Measured profile of figure 22(b).

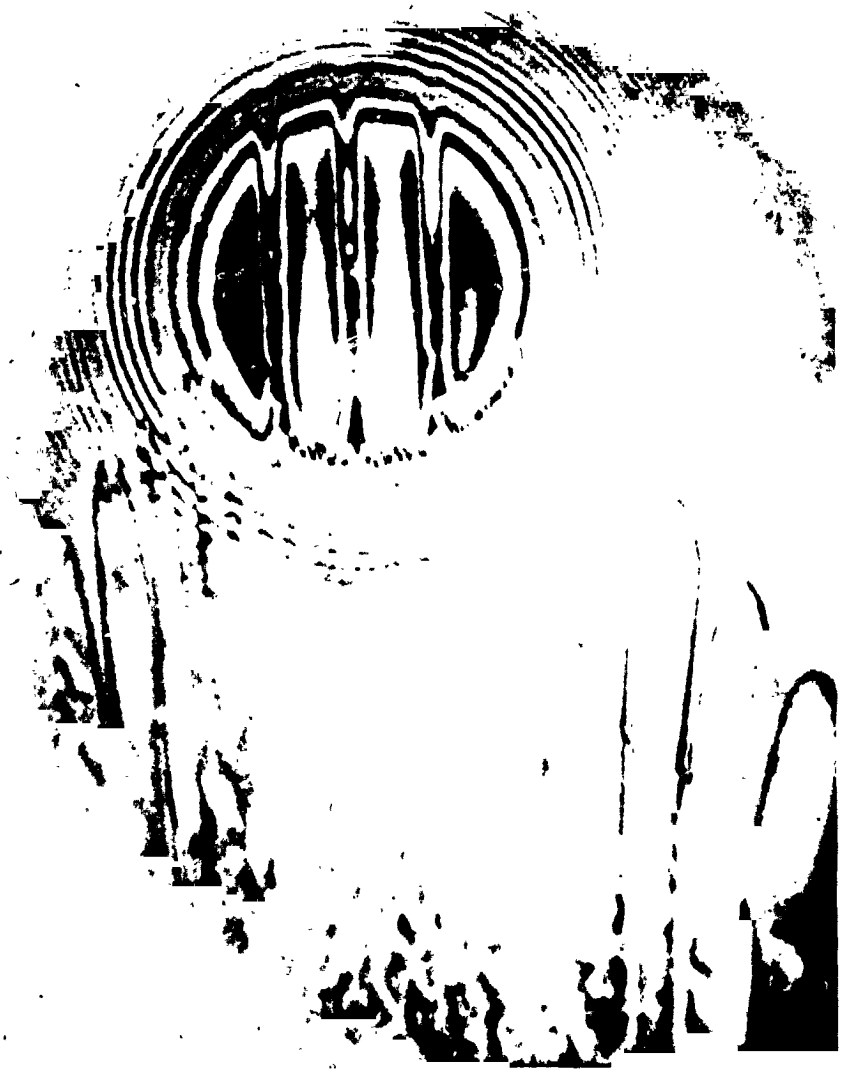

(a) PHOTOMICROGRAPH OF GROOVES UNDER SLIDING CONDITIONS. GROOVES NEAR CENTER. U = 0.0134 M/S, P_{max} = 1.13×10^9 N/M^2.

Figure 24.

(b) PHOTOMICROGRAPH OF GROOVES UNDER SLIDING CONDITIONS, GROOVES NEAR EXIT. $U = 0.0134$ M/S, $P_{max} = 1.13 \times 10^9$ N/M^2.

Figure 24. - Concluded.

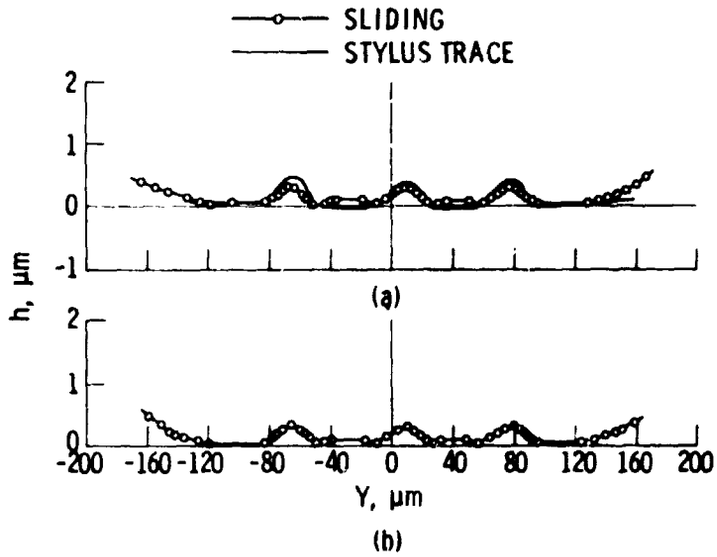

Figure 25. - (a) Comparison of measured profile of figure 24(a) and stylus trace, (b) Measured profile of figure 24(b).

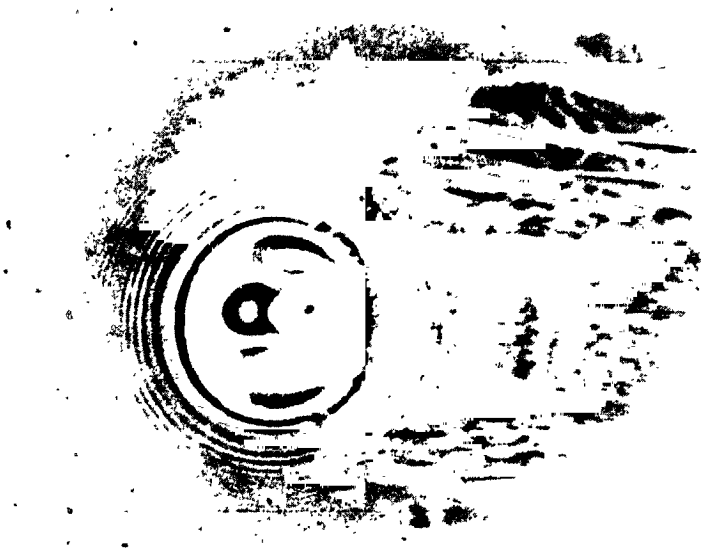

(a) PHOTOMICROGRAPH OF DENT UNDER SLIDING CONDITIONS, DENT NEAR CENTER. U = 0.0134 M/S, $P_{max} = 1.13 \times 10^9$ N/M^2.

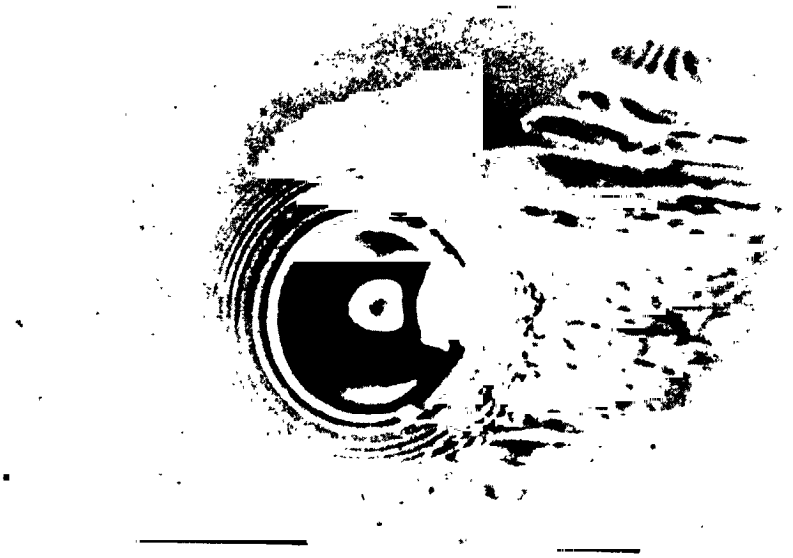

(b) PHOTOMICROGRAPH OF DENT UNDER SLIDING CONDITIONS, DENT AT EXIT. U = 0.0134 M/S, $P_{max} = 1.13 \times 10^9$ N/M^2.

Figure 26.

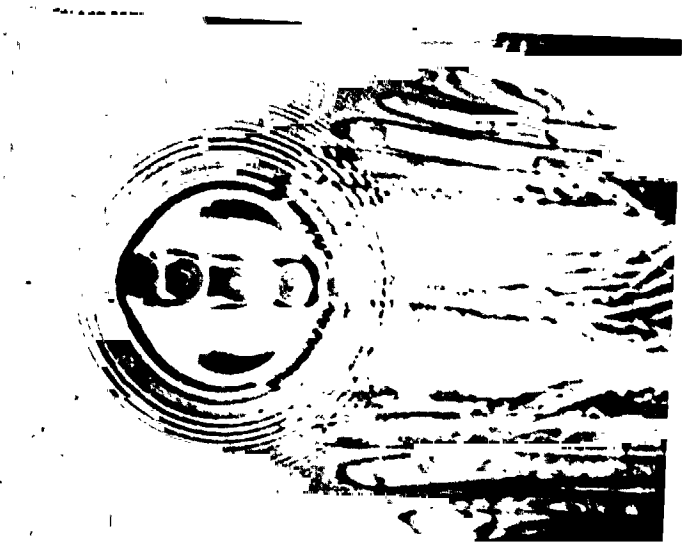

(a) PHOTOMICROGRAPH OF A SERIES OF DENTS UNDER SLIDING CONDITIONS, DENT OF INTEREST NEAR CENTER. U = 0.0134 M/S, P_{max} = 1.13×10^9 N/M^2.

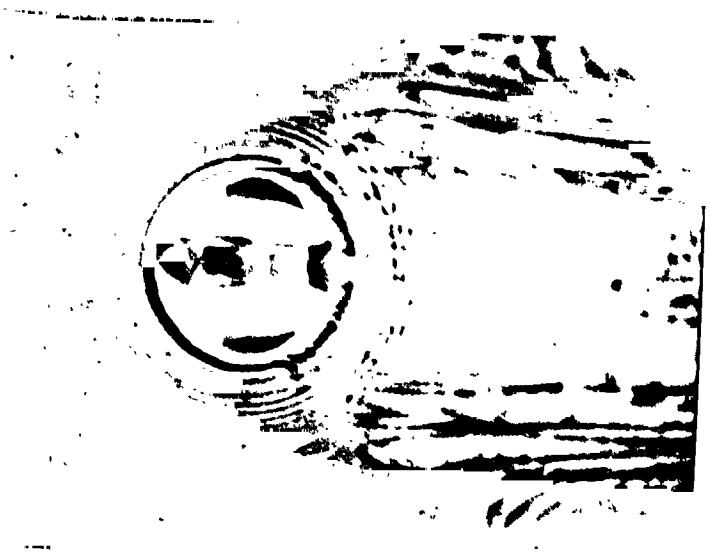

(b) PHOTOMICROGRAPH OF A SERIES OF DENTS UNDER SLIDING CONDITIONS, DENT OF INTEREST AT EXIT. U = 0.0134 M/S, P_{max} = 1.13×10^9 N/M^2.

Figure 27.

(a) PHOTOMICROGRAPH OF SINGLE GROOVE UNDER SLIDING CONDITIONS, GROOVE NEAR CENTER, U = 0.0134 M/S, P_{max} = 1.13×10^9 N/M^2.

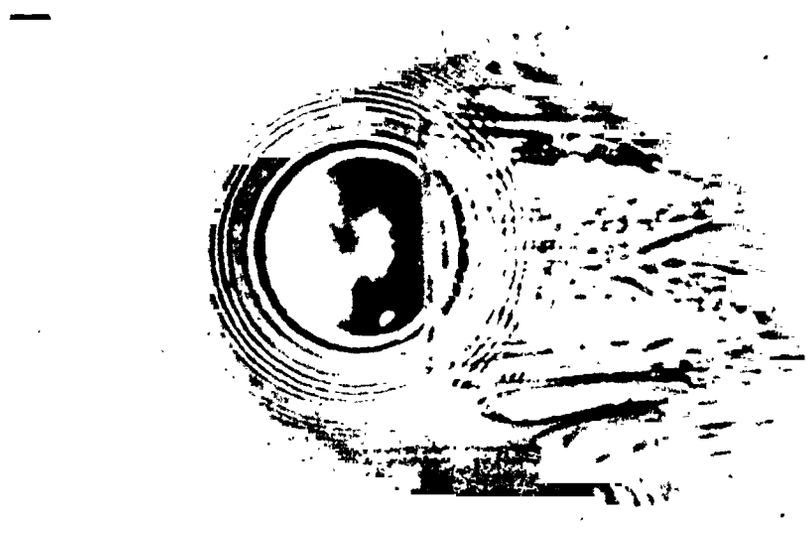

(b) PHOTOMICROGRAPH OF A SINGLE GROOVE UNDER SLIDING CONDITIONS, GROOVE AT EXIT. U = 0.0134 M/S, P_{max} = 1.13×10^9 N/M^2.

Figure 28.

(a) PHOTOMICROGRAPH OF TWO GROOVES UNDER SLIDING CONDITIONS, GROOVES NEAR CENTER. U = 0.0134 M/S, P_{max} = 1.13x10^9 N/M^2.

(b) PHOTOMICROGRAPH OF TWO GROOVES UNDER SLIDING CONDITIONS, GROOVES AT EXIT. U = 0.0134 M/S, P_{max} = 1.13x10^9 N/M^2.

Figure 29.

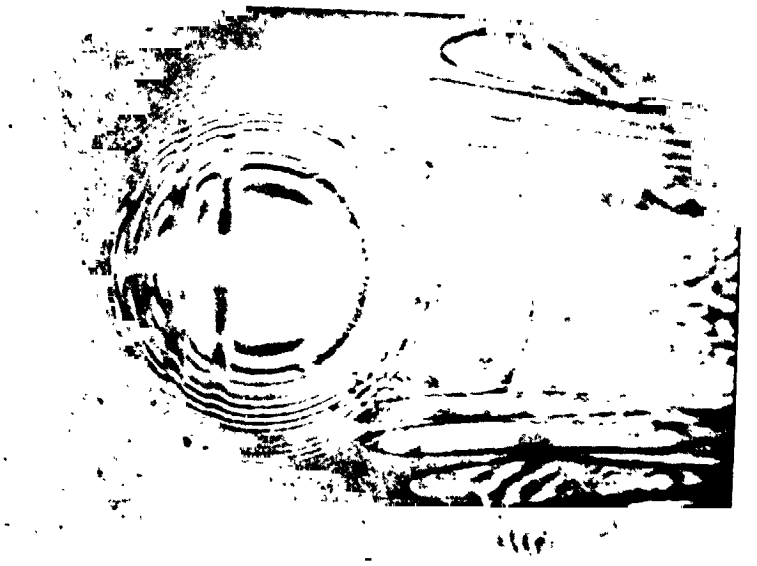

(a) PHOTOMICROGRAPH OF THREE GROOVES UNDER SLIDING CONDITIONS, GROOVES NEAR INLET. $U = 0.0134$ M/S $P_{max} = 1.13 \times 10^9$ N/M^2.

(b) PHOTOMICROGRAPH OF THREE GROOVES UNDER SLIDING CONDITIONS, GROOVES NEAR EXIT. $U = 0.0134$ M/S, $P_{max} = 1.13 \times 10^9$ N/M^2.

Figure 30.